Persistent sulfate formation from London Fog to Chinese haze

Gehui Wang[a,b,c,d,e,1], Renyi Zhang[c,d,f,2], Mario E. Gomez[c,d,g], Lingxiao Yang[c,h], Misti Levy Zamora[c], Min Hu[f], Yun Lin[c], Jianfei Peng[c,f], Song Guo[c,f], Jingjing Meng[a,b,i], Jianjun Li[a,b], Chunlei Cheng[a,b,i], Tafeng Hu[a,b], Yanqin Ren[a,b,i], Yuesi Wang[j], Jian Gao[k], Junji Cao[a,b], Zhisheng An[a,b,l], Weijian Zhou[a,b,m], Guohui Li[a,b], Jiayuan Wang[a,b,i], Pengfei Tian[c,n], Wilmarie Marrero-Ortiz[c,d], Jeremiah Secrest[c,d], Zhuofei Du[f], Jing Zheng[f], Dongjie Shang[f], Limin Zeng[f], Min Shao[f], Weigang Wang[c,o,p], Yao Huang[a,b,i], Yuan Wang[q], Yujiao Zhu[c,r], Yixin Li[c], Jiaxi Hu[c], Bowen Pan[c], Li Cai[c,s], Yuting Cheng[a,b,i], Yuemeng Ji[c,t], Fang Zhang[c,l], Daniel Rosenfeld[c,u], Peter S. Liss[c,v], Robert A. Duce[c], Charles E. Kolb[c,w], and Mario J. Molina[x,2]

[a]State Key Laboratory of Loess and Quaternary Geology, Institute of Earth Environment, Chinese Academy of Sciences, Xi'an 710061, China; [b]Key Laboratory of Aerosol Chemistry and Physics, Institute of Earth Environment, Chinese Academy of Sciences, Xi'an 710061, China; [c]Department of Atmospheric Sciences, Texas A&M University, College Station, TX 77843; [d]Department of Chemistry, Texas A&M University, College Station, TX 77840; [e]School of Geographic Sciences, East China Normal University, Shanghai 200062, China; [f]State Key Joint Laboratory of Environmental Simulation and Pollution Control, College of Environmental Sciences and Engineering, Peking University, Beijing 100871, China; [g]Department of Chemistry and Biochemistry, Florida International University, Miami, FL 33199; [h]School of Environmental Science and Engineering, Shandong University, Jinan 250100, China; [i]University of Chinese Academy of Sciences, Beijing 100049, China; [j]Institute of Atmospheric Physics, Chinese Academy of Sciences, Beijing 100029, China; [k]Chinese Research Academy of Environmental Sciences, Beijing 100000, China; [l]Beijing Normal University, Beijing 100875, China; [m]Xi'an Jiaotong University, Xi'an 710049, China; [n]Key Laboratory for Semi-Arid Climate Change of the Ministry of Education, College of Atmospheric Sciences, Lanzhou University, Lanzhou 730000, China; [o]State Key Laboratory for Structural Chemistry of Unstable and Stable Species, Institute of Chemistry, Chinese Academy of Sciences, Beijing 100190, China; [p]Beijing National Laboratory for Molecular Sciences, Institute of Chemistry, Chinese Academy of Sciences, Beijing 100190, China; [q]Jet Propulsion Laboratory, California Institute of Technology, Pasadena, CA 91125; [r]Key Laboratory of Marine Environmental Science and Ecology, Ministry of Education, Ocean University of China, Qingdao 266100, China; [s]School of Electrical Engineering, Wuhan University, Wuhan 430072, China; [t]School of Environmental Science and Engineering, Institute of Environmental Health and Pollution Control, Guangdong University of Technology, Guangzhou 510006, China; [u]Program of Atmospheric Sciences, Institute of Earth Sciences, The Hebrew University of Jerusalem, Jerusalem 91904, Israel; [v]School of Environmental Sciences, University of East Anglia, Norwich, NR4 7TJ, United Kingdom; [w]Aerodyne Research, Inc., Billerica, MA 01821-3976; and [x]Department of Chemistry and Biochemistry, University of California, San Diego, La Jolla, CA 92093

Sulfate aerosols exert profound impacts on human and ecosystem health, weather, and climate, but their formation mechanism remains uncertain. Atmospheric models consistently underpredict sulfate levels under diverse environmental conditions. From atmospheric measurements in two Chinese megacities and complementary laboratory experiments, we show that the aqueous oxidation of SO_2 by NO_2 is key to efficient sulfate formation but is only feasible under two atmospheric conditions: on fine aerosols with high relative humidity and NH_3 neutralization or under cloud conditions. Under polluted environments, this SO_2 oxidation process leads to large sulfate production rates and promotes formation of nitrate and organic matter on aqueous particles, exacerbating severe haze development. Effective haze mitigation is achievable by intervening in the sulfate formation process with enforced NH_3 and NO_2 control measures. In addition to explaining the polluted episodes currently occurring in China and during the 1952 London Fog, this sulfate production mechanism is widespread, and our results suggest a way to tackle this growing problem in China and much of the developing world.

sulfate aerosol | severe haze | pollution | human health | climate

Fine particulate matter (PM), which typically contains a complex mixture of inorganic and organic species, has important implications for several environmental issues (1–3). Presently, the mechanisms leading to PM formation remain uncertain, particularly under highly polluted conditions, hindering efforts in developing effective mitigation policies to reduce their local, regional, and global impacts (1). It is well established, though, that sulfate (SO_4^{2-}) is ubiquitous and is a key PM constituent in the atmosphere. Moreover, hygroscopic sulfate aerosols serve as efficient cloud condensation nuclei, affecting cloud formation, precipitation, and climate (4–8). A major fraction of regional acid deposition is attributed to the sulfate content that exerts debilitating effects on acid-sensitive ecosystems (9). Furthermore, high levels of fine PM have been implicated in adverse human health issues (1), as exemplified by high fatality during the 1952 London Fog (1, 10). Sulfur compounds are emitted globally from many natural and anthropogenic sources (1–3, 11),

and there have been high SO_2 emissions from combustion of coal and petroleum products in developing countries (such as China) spurred on by fast economic development (12).

Gaseous SO_2 is converted to particulate sulfate through gas-phase oxidation or aqueous reactions, but the detailed chemical mechanisms remain controversial (1–3, 13, 14). The gas-phase

Significance

Exceedingly high levels of fine particulate matter (PM) occur frequently in China, but the mechanism of severe haze formation remains unclear. From atmospheric measurements in two Chinese megacities and laboratory experiments, we show that the oxidation of SO_2 by NO_2 occurs efficiently in aqueous media under two polluted conditions: first, during the formation of the 1952 London Fog via in-cloud oxidation; and second, on fine PM with NH_3 neutralization during severe haze in China. We suggest that effective haze mitigation is achievable by intervening in the sulfate formation process with NH_3 and NO_2 emission control measures. Hence, our results explain the outstanding sulfur problem during the historic London Fog formation and elucidate the chemical mechanism of severe haze in China.

oxidation of SO_2 is dominated by its reaction with the OH radical, with a lifetime of ~1 wk at the typical tropospheric level of OH radicals. The aqueous pathways of SO_2 oxidation may occur much faster, including reactions with dissolved ozone, hydrogen peroxide, organic peroxides, OH, and NO_2 via catalytic or non-catalytic pathways involving mineral oxides (15–20). Most recently, an interfacial SO_2 oxidation mechanism involving O_2 on acidic microdroplets has been suggested (16).

It has been hypothesized that aqueous SO_2 oxidation by NO_2 can be an important pathway for sulfate formation under urban conditions and in the presence of sufficient neutralizing agents such as NH_3 (2). Several earlier experimental studies, in which gaseous NO_2 was exposed to bulk solutions containing sulfite (SO_3^{2-}) and hydrogen sulfite (HSO_3^-) ions prepared from Na_2SO_3, investigated the aqueous sulfur oxidation by NO_2; the measured rate constants differed by 1–2 orders of magnitude (17–19). Typically, this aqueous oxidation has been neglected in atmospheric models because of limited water solubility of NO_2 (1, 13, 20). A model simulation of dissolution of NO_2 in cloud droplets under NO_x-rich environments has shown enhanced regional wintertime sulfate by up to 20%, resulting in better agreement between simulations and observations (13). Also, atmospheric measurements have revealed high sulfate production during severe haze events in China (21–25), which cannot be explained by current atmospheric models and suggests missing sulfur oxidation mechanisms (14). Typically, high sulfate levels during haze events in China occurred with concurrently elevated RH, NO_x, and NH_3 (24, 25), implicating an aqueous sulfur oxidation pathway. However, elucidation of the sulfur oxidation mechanisms from available atmospheric measurements remains challenging, particularly under polluted conditions because of multiple highly coemitted primary gaseous pollutants (1, 21). In this work we investigated the sulfur oxidation mechanism and its role in severe haze formation, by combining field measurements of gaseous pollutants and aerosol particle properties in two Chinese megacities (Xi'an and Beijing) and complementary laboratory experiments (*Materials and Methods* and *SI Appendix*).

Results

Sulfate Evolution During Pollution Episodes. The pollution episodes in Xi'an exhibit a periodic cycle of 4–5 d, which is reflected in the temporal evolutions of the mass concentrations of SO_4^{2-} and PM

smaller than 2.5 μm ($PM_{2.5}$) (Fig. 1*A* and *SI Appendix*, Fig. S1*A* and Table S1). For each pollution episode, the SO_4^{2-} mass concentration increases markedly from less than 10 μg m^{-3} (clean), 10–20 μg m^{-3} (transition), to greater than 20 μg m^{-3} (polluted), with the corresponding increases in the mean $PM_{2.5}$ mass concentrations from 43, 139, to 250 μg m^{-3}, respectively. Among the main non-refractory $PM_{2.5}$ species in Xi'an (Fig. 1*B*), organic matter (OM), nitrate (NO_3^-), and SO_4^{2-} are most abundant throughout the pollution episode. The SO_4^{2-} mass fraction increases during the transition and polluted (hazy) periods, whereas there is a slight decrease in the OM mass fraction. We quantified the molar ratio of SO_4^{2-} to SO_2, which reflects sulfur partitioning between the particle and gas phases. This ratio ranges from less than 0.1 at relative humidity (RH) <20% to 1.1 at RH >90% in Xi'an, exhibiting an exponential increase with RH (Fig. 1*C*). During the pollution development, there is increasing RH (Fig. 1*D* and *SI Appendix*, Fig. S1*B*), and the concentrations of SO_2, NO_x (NO + NO_2), and NH_3 are highly elevated (Fig. 1*D* and *SI Appendix*, Fig. S2 *A–C*). Clearly, the larger conversion of SO_2 to SO_4^{2-} during the hazy periods is responsible for the enhanced SO_4^{2-} formation, i.e., with high mass concentrations and mass fractions (Fig. 1 *A* and *B*). Field measurements in Beijing also show a similar SO_4^{2-} evolution. There are noticeable increases in SO_4^{2-} and $PM_{2.5}$ mass concentrations during the pollution development (Fig. 1*E* and *SI Appendix*, Fig. S3*A* and Table S2). The SO_4^{2-} mass fraction increases from clean to polluted periods, in contrast to a decreasing OM mass fraction (Fig. 1*F*). During the hazy periods in Beijing, the molar ratio of SO_4^{2-} to SO_2 also exhibits an exponential increase with RH (Fig. 1*G*), and RH and the concentrations of SO_2, NO_x, and NH_3 are high (Fig. 1*H* and *SI Appendix*, Figs. S3*B* and S4 *A–C*).

Our field measurements demonstrate that efficient conversion of SO_2 to SO_4^{2-} occurs at high RH and concurrently with elevated concentrations of SO_2, NO_x, and NH_3, implicating aqueous sulfate production from the participation of these species. Furthermore, the enhanced sulfate formation during the hazy periods is also accompanied by simultaneously increased formation of particulate NO_3^- and OM (*SI Appendix*, Fig. S5). The concentration of ozone is low during the hazy periods in both locations (i.e., a few parts per billion in *SI Appendix*, Figs. S2*D* and S4*D* and Tables S1 and S2), and the visibility is considerably reduced (*SI Appendix*, Figs. S1*C* and S3*C* and Tables S1 and S2),
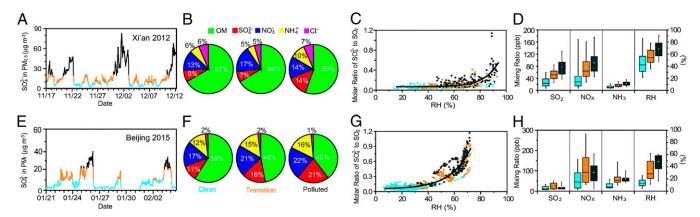
Fig. 1. Sulfate production during pollution episodes in Xi'an and Beijing. (*A–D*) Measurements in Xi'an from 17 November to 12 December 2012, and the particle properties correspond to those in $PM_{2.5}$. (*E–H*) Measurements in Beijing from 21 January to February 4, 2015, and the particle properties correspond to those in PM_1 (particles smaller than 1 μm). In *A* and *E*, the dates on the x axis correspond to midnight local time. *B* and *F* show the mass fractions of the five main nonrefractory constituents from 5 to 12 December 2012 in Xi'an and from 21 January to 4 February 2015 in Beijing, respectively. The lines in *C* and *G* represent the exponential fits through the data, i.e., $y = 0.07 + 1.0 \times 10^{-4} \exp(x/11)$ with $R^2 = 0.60$ in Xi'an and $y = 0.05 + 7.0 \times 10^{-3} \exp(x/15)$ with $R^2 = 0.88$ in Beijing. Except for the colors in *B* and *F* depicting the aerosol compositions, the blue, orange, and black colors correspond to the SO_4^{2-} mass concentrations of less than 10 μg m^{-3} (clean), 10–20 μg m^{-3} (transition), and greater than 20 μg m^{-3} (polluted), respectively. The top and bottom of the vertical line for each box in *D* and *H* correspond to the 95th and 5th percentiles, respectively, and the top, middle, and bottom horizontal lines of the box mark the 75th, 50th, and 25th percentiles of the data range. The white dot in each box represents the mean value.

both indicating weak photochemical activity (26, 27). Further examination of the measurements in Beijing reveals markedly continuous growths in the $PM_{2.5}$ mass concentration and the average particle size throughout the pollution episodes (*SI Appendix*, Fig. S6 *A and C*), which are attributable to efficient formation of SO_4^{2-}, NO_3^-, and secondary organic aerosol (SOA) during the hazy periods. The considerably reduced photochemical activity during the hazy periods is also reflected in the measured decrease in the photolysis rate coefficient of NO_2 (J_{NO2}) (*SI Appendix*, Fig. S6*B*), evident from the anticorrelation between J_{NO2} and $PM_{2.5}$. Clearly, the efficient PM mass and size growths at high RH and low photochemical activity during the hazy periods are indicative of an increasing importance of aqueous phase oxidation not only for SO_4^{2-} but also for NO_3^- and SOA.

A comparison between the two field studies reveals some distinctions. For example, the ratio of SO_4^{2-} to SO_2 at 70% RH is 0.8 in Beijing, much larger than the corresponding value of 0.1 in Xi'an. In addition, the SO_4^{2-} mass fraction and the total inorganic mass fraction in Beijing are larger than those in Xi'an, indicating that fine PM is more hygroscopic in Beijing (21). The measured contents of Fe and Mn of fine PM are small during the hazy periods in Xi'an (*SI Appendix*, Table S1), consistent with size-resolved composition measurements showing that the mineral elements are usually enriched in coarse particles, because of their dust origins in China (1, 21, 23). With negligibly low concentrations of water-soluble Fe and Mn (*SI Appendix*, Table S1), the catalytic capability of the mineral elements in fine PM is limited.

Ammonia Neutralization. To evaluate the PM acidity during the field campaigns, we calculated the equivalent ratio of ammonium (NH_4^+) to the sum of SO_4^{2-} and NO_3^- (*SI Appendix*, Fig. S7), because these species represent the dominant nonproton cations and anions in fine PM, respectively. During the hazy periods in Xi'an, this ratio remains near unity (Fig. 2*A*). Hence, SO_4^{2-} and NO_3^- in fine PM are completely neutralized, because of the presence of high levels of gaseous ammonia (17–23 parts per billion, ppb) during the hazy periods. Further analysis of the $PM_{2.5}$ chemical compositions reveals that the equivalent ratio of the total nonproton cations (NH_4^+, Na^+, Ca^{2+}, Mg^{2+}, and K^+) to anions (SO_4^{2-}, NO_3^-, and Cl^-) is also near unity (Fig. 2*B* and *SI Appendix*, Fig. S8*A*), with the mean values of 1.15 ± 0.14 and 1.06 ± 0.06 during the transition and polluted periods, respectively. The close balance between these cations and anions in Xi'an further confirms that fine PM exhibits negligible acidity. Similarly, the equivalent ratio of NH_4^+ to SO_4^{2-} and NO_3^- is slightly larger than unity throughout the pollution episodes in Beijing (Fig. 2*A* and *SI Appendix*, Fig. S7*B*). When the chloride anion, which likely exists as NH_4Cl in ambient PM, is included, the ratio is reduced to 1.09 ± 0.11 during the polluted period (Fig. 2*B* and *SI Appendix*, Fig. S8*B*). Hence, fine PM in both locations is effectively neutralized by ammonia with a calculated pH ~7 (*SI Appendix*, Tables S1 and S2), when rapid sulfate production occurs during the polluted period. Interestingly, our results of fully neutralized fine PM in China are in contrast to a recent study showing highly acidic aerosols in the southeast United States, despite declining atmospheric sulfate concentrations over the past 15 years (28).

An Aqueous Synergetic SO_2 Oxidation Pathway. To elucidate the mechanism of SO_2 oxidation and interpret the rapid sulfate production in our field measurements, we conducted a series of laboratory experiments by exposing pure water or ammonium (3 wt %) solutions under dark conditions to gaseous SO_2 and NO_2 in a reaction cell. Sulfate formation was quantified (SO_4^{2-} at $m/z = 96$, *SI Appendix*, Fig. S9*A*) by thermal desorption-ion drift-chemical ionization mass spectrometry (TD-ID-CIMS) (29, 30). When the pure water or ammonium solutions were exposed simultaneously to SO_2 and NO_2 using either N_2 or air as the buffer gas, significant SO_4^{2-} production was detected, and the signal was higher in the ammonium solution than in pure water
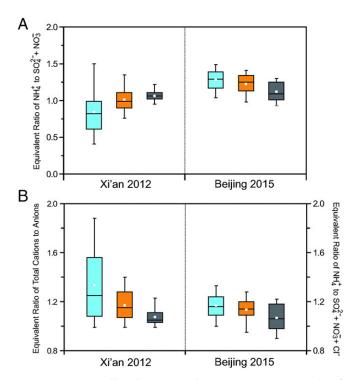

Fig. 2. Neutralizing effect of ammonia on fine PM. (*A*) Equivalent ratio of NH_4^+ to the sum of SO_4^{2-} and NO_3^- in Xi'an and Beijing. (*B*) Equivalent ratio of the total cations to anions in Xi'an and equivalent ratio of NH_4^+ to the sum of SO_4^{2-}, NO_3^-, and Cl^- in Beijing. The blue, orange, and black colors correspond to the clean, transition, and polluted periods, respectively, as defined in Fig. 1.

(*SI Appendix*, Table S3). In contrast, the SO_4^{2-} production was absent for only SO_2 exposure under similar conditions, indicating the oxidizing role of NO_2. Also, there was little difference in the measured SO_4^{2-} production between experiments using N_2 and air, suggesting negligible SO_2 oxidation by O_2 molecules.

We performed additional experiments by exposing seed particles to gaseous SO_2, NO_2, and NH_3 under dark and variable RH conditions in a reaction chamber (*SI Appendix*, Fig. S10). Size-selected oxalic acid particles, which were used to represent organic aerosols that dominate the early stages of haze development in China (21) (see also Fig. 1 *B* and *F*), were simultaneously exposed to SO_2, NO_2, and NH_3, while the variation in the dry particle size was monitored. The evolution in particle size distributions measured after exposure to three different RH conditions is depicted in Fig. 3*A*: The size distribution remains unchanged at 30% RH (i.e., identical to that of the initially seeded particles), whereas exposures at 60% and 70% RH lead to dramatic shifts to larger size distributions. We also conducted experiments to analyze the chemical composition of exposed particles. SO_4^{2-} production in collected particles after the exposure at high RH is clearly evident (Fig. 3*B* and *SI Appendix*, Fig. S9*B*).

We quantified the growth of seed particles after exposure to SO_2, NO_2, and NH_3, on the basis of the measured ratio of the dry particle sizes (D_p/D_o), where D_p and D_o are the values after and before the exposure, respectively. The growth factor increases with RH, with the values of near unity (no growth) at RH< 20% and 2.3 at 70% RH (Fig. 3*C*). The size growth after exposure is explained by SO_4^{2-} production, as depicted in the corresponding increase of the integrated SO_4^{2-} desorption peak areas (Fig. 3*D*). Both the particle size growth and the SO_4^{2-} formation after the exposure to SO_2, NO_2, and NH_3 display a similar exponential increase with RH, consistent with increasing hygroscopic growth of oxalic acid particles (31). We performed additional measurements when one or both of NO_2 and NH_3 were excluded from the exposure: In the absence of NO_2, NH_3, or
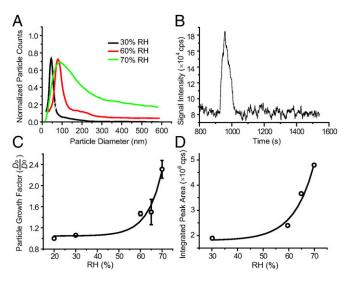
Fig. 3. Aqueous sulfate formation in the reaction chamber. (*A*) Evolution in the dry particle size distribution when sized selected oxalic acid particles are exposed to SO$_2$, NO$_2$, and NH$_3$ under three different RH conditions in a 1-m^3 reaction chamber. (*B*) Desorption spectra of particles collected by TD-ID-CIMS after exposure to SO$_2$, NO$_2$, and NH$_3$ at 65% RH. (*C*) Particle growth factor after exposure to SO$_2$, NO$_2$, and NH$_3$ as a function of RH. The exponential fit is $y = 1.05 + 4.0 \times 10^{-5}$ exp (x/6.8) with $R^2 = 0.96$. Each point corresponds to three measurements, and the error bar denotes the SD (1σ). (*D*) Integrated desorption peak areas of particles collected by TD-ID-CIMS after exposure to SO$_2$, NO$_2$, and NH$_3$ as a function of RH. The exponential fit is $y = 1.8 \times 10^6 + 417$exp ($x$/7.9) with $R^2 = 0.97$. All experiments were performed under the dark condition and at temperature of 298 K. The exposure time was 60 min, and the initial particle size was 45 nm. The initial gas concentrations were 250 ppb for SO$_2$ and NO$_2$ and 1 ppm for NH$_3$.

both from the exposure, no observable particle growth or SO$_4^{2-}$ production was measured (*SI Appendix*, Table S4).

On the basis of our combined field and laboratory measurements, we establish the occurrence of an overall aqueous reaction between SO$_2$ and NO$_2$,

$$SO_2(g) + 2NO_2(g) + 2H_2O(aq) \rightarrow 2H^+(aq) + SO_4^{2-}(aq)$$

$$+ 2HONO(g). \quad [1]$$

Because this reaction is second order with respect to NO$_2$ accommodation, its rate is strongly dependent on the gaseous NO$_2$ concentration, i.e., only proceeding efficiently under NO$_2$-rich conditions. This reaction is also dependent on pH, which not only governs the solubility but also the aqueous reaction rate. For example, when the pH value is varied from 6 to 4, the effective Henry's constant of SO$_2$ decreases by more than two orders of magnitude (1–3), leading to a decreased oxidation rate of approximately two orders of magnitude (17–19). In addition, the solubility is dependent of temperature, i.e., increasing with decreasing temperature (32–34). Also, the reaction is self-limiting because of the acidity effect, namely that its occurrence increases acidity in the aqueous phase and in turn reduces the solubility and reaction rate. Nitrous acid (HONO) generated from this reaction is likely released into the gas phase because of its limited solubility in aqueous solution (34). The measurements in Xi'an show that the HONO concentration increases during the pollution development, reaching 2–3 ppb during the hazy periods (*SI Appendix*, Fig. S11A). Also, the measured HONO concentration is correlated with increasing RH but is inversely correlated with gaseous SO$_2$, likely supporting its formation from the aqueous SO$_2$ oxidation by NO$_2$ (*SI Appendix*, Fig. S11B). The previously proposed HONO formation mechanisms include heterogeneous conversion of NO$_2$ on ground or aerosol surfaces (1–3).

Our results indicate that aqueous SO$_2$ oxidation by NO$_2$ is favored in two atmospheric scenarios (Fig. 4), i.e., under cloud/fog conditions and on fine aerosols with high RH (> 60–70%) and sufficient neutralization (pH ∼ 7). In-cloud SO$_2$ oxidation proceeds in the presence or absence of a neutralizing agent, when elevated levels of SO$_2$ and NO$_2$ coexist (Fig. 4*A*). Cloud droplets are large (exceeding several tens of micrometers in sizes), and the amount of sulfate formed is sufficiently diluted and does not appreciably alter the particle acidity (1–3). Consequently, water evaporation from cloud droplets under unsaturated conditions leads to concentrated sulfuric acid particles (33), contributing to acid rain and regional acid deposition (9, 13). Also, in-cloud SO$_2$ oxidation can be further enhanced in the presence of the basic species, as demonstrated in our laboratory work for NH$_3$ (*SI Appendix*, Table S3). On the other hand, the oxidation on fine PM is inhibited by the acidity effect, and the presence of basic species (i.e., NH$_3$) is necessary to maintain the oxidation (Fig. 4*B*),

$$2NH_3(g) + SO_2(g) + 2NO_2(g) + 2H_2O(aq) \rightarrow 2NH_4^+(aq)$$

$$+ SO_4^{2-}(aq) + 2HONO(g). \quad [2]$$

The acidity effect is relevant to the ionic strength, which is highly dependent on the particle size, i.e., decreasing by two to four orders of magnitude from submicrometer aerosols to cloud droplets (1–3, 35). Note that this acidity effect on aerosol sulfate formation (i.e., decreasing with increasing particle size) is analogous to the Kelvin (curvature) effect, which represents a major barrier in aerosol nucleation (36, 37). In addition, neutralization of fine PM can be facilitated by amines, albeit at a lower atmospheric concentration than NH$_3$ (38, 39).
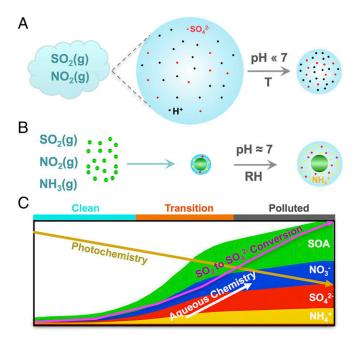
Fig. 4. Schematic of the sulfate formation mechanisms. Variations in temperature, RH, and particle size and acidity for the aqueous reactions between SO$_2$ and NO$_2$ leading to SO$_4^{2-}$ formation under in-cloud conditions (*A*) and on fine PM (*B*). The red, black, yellow, and green colors in *A* and *B* represent SO$_4^{2-}$, H$^+$, NH$_4^+$, and SOA, respectively. (*C*) Anticorrelation between the photochemical activity and aqueous chemistry during the severe haze evolution (i.e., from the clean, transition, to polluted periods) in China, displaying the central role of the SO$_2$ to SO$_4^{2-}$ conversion in facilitating aqueous production of the major secondary constituents.

Hence, the acidity, hygroscopicity, and RH represent the key factors for sulfate formation on fine PM, explaining the differences in the various ambient measurements (14, 20–25). For example, the acidity effect on fine aerosols is effectively overcome by NH_3 neutralization in Xi'an and Beijing (Fig. 2). Also, the noticeably earlier increase of the SO_4^{2-} to SO_2 ratio with RH in Beijing than in Xi'an (Fig. 1 *C* and *G*) is attributable to more hygroscopic aerosols, because of a larger inorganic mass fraction in Beijing (Fig. 1 *B* and *F*) (21).

We derived the equivalent SO_2 uptake coefficient (γ) for sulfate production from our field and laboratory results in *SI Appendix*, Tables S5 and S6, respectively. The γ-values derived from the Beijing measurements are $(2.1 \pm 1.6) \times 10^{-5}$ and $(4.5 \pm 1.1) \times 10^{-5}$ during the transition (41% RH) and polluted (56% RH) periods, respectively, compared with $(8.3 \pm 5.7) \times 10^{-5}$ at 65% RH and $(3.9 \pm 1.2) \times 10^{-4}$ at 70% RH derived from the laboratory measurements. Hence, our laboratory experiments reproduce the rapid sulfate production measured under polluted ambient conditions, and these kinetic data are applicable for quantifying sulfate formation in atmospheric models (1, 13, 14).

The Central Role of Sulfate Production in Severe Haze Development. Our results indicate that the formation of the various secondary organic and inorganic constituents in fine PM is mutually promoting and the severe haze development involves a transition from photochemical to aqueous phase processes (Fig. 4*C*). During the early stage, efficient photochemical oxidation of volatile organic compounds (VOCs) leads to SOA formation (Fig. 1 *B* and *F*), which provides an aqueous media for subsequent SO_4^{2-} production. With high RH and low photochemical activity during the later hazy periods, continuously large PM growth (i.e., the SO_4^{2-}, NO_3^-, and OM mass increases) is maintained by the aqueous chemistry (*SI Appendix*, Fig. S5). In particular, the SO_4^{2-} production likely represents the most critical step in initializing the aqueous chemistry, because of increasing particle hygroscopicity. Efficient SO_2 to SO_4^{2-} conversion not only contributes to the high SO_4^{2-} production rate, but also enhances formations of NO_3^- and SOA on aqueous particles, explaining the sustained high production of the major secondary constituents during the hazy periods in our current field measurements and those of the previous studies in China (1, 21, 40). For example, with reduced photochemistry during the hazy periods, the measured large NO_3^- mass concentration is attributable to an enhanced heterogeneous conversion of NO_x to HNO_3, because the hydrolysis reaction of N_2O_5 occurs efficiently on sulfate aerosols (41). Also, hydration and oligomerization reactions of glyoxal and methylglyoxal, which are produced with high yields by aromatic hydrocarbon oxidation from traffic emissions, are enhanced by sulfate formation, because these reactions are highly dependent on particle hygroscopicity (30, 32, 42). Furthermore, gaseous HONO formed from the aqueous SO_2 oxidation with NO_2 provides an additional photochemical OH source that enhances the atmospheric oxidizing capability during the hazy periods (43). It should also be pointed out that severe haze formation in China is characterized by a complex interplay between meteorological, thermodynamic, and chemical processes (1, 21, 44).

Conclusion

Atmospheric sulfur chemistry has remained an open problem (1, 13, 14). The formation of the 1952 London "Killer" Fog is still mysterious in terms of the detailed chemical mechanism for SO_2 conversion to sulfate (1, 45). Our results indicate that the formation of London Fog was similar to in-cloud SO_2 oxidation by NO_2 (Fig. 4*A*), because both species were present in highly elevated levels as the coproducts of coal burning. The sulfate formation was greatly facilitated by high RH, low temperature, and the presence of large fog droplets (45), yielding elevated sulfuric acid levels that persisted throughout the event. The particle acidity was regulated by temperature, and water evaporation from fog droplets at warmer

temperature resulted in concentrated sulfate acid particles (33), explaining the highly acidic nature of the London Fog (45).

Interestingly, we show that the same sulfur problem persists presently to contribute to severe haze formation in China, although the fine PM is mainly nonacidic. Major emission sources in China include industry (for SO_2, VOCs, and NO_x) and traffic (for VOCs and NO_x), because of its fast-growing economy and urbanization (1, 23, 46, 47). Also, there has been a rapid increase in the production and use of nitrogen fertilizers in China, leading to high NH_3 emissions (48). For example, the emissions of SO_2, NO_x, and NH_3 in China are estimated to be about 22 Tg S y^{-1}, 19 Tg N y^{-1}, and 15 Tg N y^{-1} in 2010, respectively (48). In addition, traffic emissions have been suggested to represent an important urban NH_3 source (49). High emissions of these organic and inorganic PM precursors result in large secondary production of SO_4^{2-}, NO_3^-, NH_4^+, and SOA in China (Fig. 4*C*), via the combined atmospheric photochemical and aqueous processes (1, 21, 40, 50–53). Our results indicate that sulfate production is key to the formation of persistent severe haze in China (Fig. 4 *B* and *C*). Whereas current efforts have been focused primarily on minimizing SO_2 emissions (1, 14, 21), significant haze reduction may only be achievable by disrupting this sulfate formation process. For example, controlled NH_3 emissions may be important, because the acidity effect represents the key rate-limiting factor in sulfate production on fine PM. Also, because of the second-order nature of NO_2 in the aqueous SO_2 oxidation (i.e., reactions **1** and **2**), reduction of the NO_x level is likely effective in lowering sulfate formation. In light of large contributions to urban NO_x, VOC, and NH_3 levels from transportation (1, 21, 49), regulatory actions in minimizing traffic emissions may represent the critical step in mitigating severe haze in China. These measures are clearly supported by our experimental results, showing no particle growth or sulfate formation at high RH when oxalic acid particles were exposed to high levels of SO_2 in the absence of NH_3, NO_2, or both (*SI Appendix*, Table S4).

In addition to polluted urban areas, efficient sulfate production is also expected in the proximity of power plant and biomass burning plumes and ship tracks (1–3, 9, 13), where SO_2 and NO_x are coemitted. Because of increasingly high SO_2, NO_x, VOC, and basic species (NH_3 and amine) emissions in many developing countries (1, 38, 48, 49), the synergetic sulfate formation pathway identified in our work is likely widespread globally, contributing not only to air quality problems but also to enhanced nitrogen (i.e., NH_4^+ or NO_3^-) or acid (in the absence of basic species) deposition, with major implications for the ecosystem vitality, greenhouse gas budgets, and biological diversity (48). Our results highlight the necessity for comprehensive understanding of the atmospheric aerosol chemistry in the development of effective pollution mitigation policies (1), to minimize the impacts of fine PM on visibility, human health, ecosystems, weather, and climate.

Materials and Methods

Field measurements of gaseous and PM pollutants were performed in Xi'an and Beijing. The sampling site in Xi'an (from 17 November to 12 December 2012) was located on the rooftop (around 10 m above the ground) of a three-story building on the campus of the Institute of Earth Environment of Chinese Academy of Science (CAS) in the southwest of the city (54). The sampling site in Beijing (from 21 January to 4 February 2015) was located on the campus of Peking University in northwestern Beijing (21). Gaseous species and PM properties were monitored by a suite of instrumentations and methods (54–64). Laboratory experiments were performed to evaluate SO_2 oxidation by NO_2 on bulk solutions and aerosols under dark conditions (see also *SI Appendix*). Pure water or 3 wt % NH_3 solution was exposed to SO_2 and NO_2 in N_2 or pure air using a reaction cell. The exposed solution from the reaction cell was analyzed by TD-ID-CIMS for sulfate formation. To evaluate the conversion of SO_2 into SO_4^{2-} on aerosols under conditions relevant to the atmosphere, we conducted experiments by exposing seed particles to SO_2, NO_2, and NH_3 and measuring the size variation and sulfate formation on the exposed particles in a 1-m^3 Teflon reaction chamber covered with aluminum foil (*SI Appendix*, Fig. S10). Size-selected oxalic acid particles (45 nm) were used as model aerosols in the reaction

chamber for the aqueous conversion of SO_2 to sulfate, by exposing to SO_2, NO_2, and NH_3 at variable RH. The variations in the dry particle sizes and sulfate formation were measured by a differential mobility analyzer and TD-ID-CIMS, respectively. Additional descriptions of the instrumentation and procedures of the field and laboratory measurements are provided in *SI Appendix*.

1. Zhang R, et al. (2015) Formation of urban fine particulate matter. *Chem Rev* 115(10): 3803–3855.
2. Seinfeld JH, Pandis SN (2006) *Atmospheric Chemistry and Physics: From Air Pollution to Climate Change* (John Wiley & Sons, Hoboken, NJ).
3. Finlayson-Pitts BJ, Pitts JN, Jr (1999) *Chemistry of the Upper and Lower Atmosphere: Theory, Experiments, and Applications* (Academic, San Diego).
4. Stocker TF, et al., eds (2013) *Intergovernmental Panel on Climate Change. Climate Change 2013: The Physical Science Basis. Contribution of Working Group I to the Fifth Assessment Report of the Intergovernmental Panel on Climate Change* (Cambridge Univ Press, New York), pp 571–657.
5. Zhang R, Li G, Fan J, Wu DL, Molina MJ (2007) Intensification of Pacific storm track linked to Asian pollution. *Proc Natl Acad Sci USA* 104(13):5295–5299.
6. Wu G, et al. (2015) Advances in studying interactions between aerosols and monsoon in China. *Sci China Earth Sci* 58:1–16.
7. Li G, Wang Y, Zhang R (2008) Implementation of a two-moment bulk microphysics scheme to the WRF model to investigate aerosol-cloud interaction. *J Geophys Res* 113:D15211.
8. Wang Y, et al. (2011) Long-term impacts of aerosols on precipitation and lightning over the Pearl River Delta megacity area in China. *Atmos Chem Phys* 11:12421–12436.
9. Chang JS, et al. (1987) A three-dimensional Eulerian acid deposition model: Physical concepts and formulation. *J Geophys Res* 92:14681–14700.
10. Stone R (2002) Air pollution. Counting the cost of London's killer smog. *Science* 298(5601):2106–2107.
11. Watson AJ, Upstill-Goddard RC, Liss PS (1991) Air–sea gas exchange in rough and stormy seas measured by a dual-tracer technique. *Nature* 349:145–147.
12. Lu Z, et al. (2010) Sulfur dioxide emissions in China and sulfur trends in East Asia since 2000. *Atmos Chem Phys* 10:6311–6331.
13. Sarwar G, et al. (2013) Potential impacts of two SO_2 oxidation pathways on regional sulfate concentrations: Aqueous-phase oxidation by NO_2 and gas-phase oxidation by Stabilized Criegee Intermediates. *Atmos Environ* 68:186–197.
14. Wang Y, et al. (2014) Enhanced sulfate formation during China's severe winter haze episode in January 2013 missing from current models. *J Geophys Res* 119:10,425–10,440.
15. He H, et al. (2014) Mineral dust and NO_x promote the conversion of SO_2 to sulfate in heavy pollution days. *Sci Rep* 4:4172.
16. Hung H-M, Hoffmann MR (2015) Oxidation of gas-phase SO_2 on the surfaces of acidic microdroplets: Implications for sulfate and sulfate radical anion formation in the atmospheric liquid phase. *Environ Sci Technol* 49(23):13768–13776.
17. Lee YN, Schwartz SE (1983) Kinetics of oxidation of aqueous sulfur (IV) by nitrogen dioxide. *Precipitation Scavenging, Dry Deposition and Resuspension*, eds Pruppacher HR, Semonin RG, Slinn WGN (Elsevier, New York), Vol 1, pp 453–466.
18. Huie RE, Neta P (1986) Kinetics of one-electron transfer reactions involving chlorine dioxide and nitrogen dioxide. *J Phys Chem* 90:1193–1198.
19. Clifton CL, Altstein N, Huie RE (1988) Rate constant for the reaction of nitrogen dioxide with sulfur(IV) over the pH range 5.3-13. *Environ Sci Technol* 22(5):586–589.
20. Xue J, Yuan Z, Yu JZ, Lau AKH (2014) An observation-based model for secondary inorganic aerosols. *Aerosol Air Qual Res* 14:862–878.
21. Guo S, et al. (2014) Elucidating severe urban haze formation in China. *Proc Natl Acad Sci USA* 111(49):17373–17378.
22. Sun YL, et al. (2013) Aerosol composition, sources and processes during wintertime in Beijing, China. *Atmos Chem Phys* 13:4577–4592.
23. Tian SL, Pan YP, Wang Y (2016) Size-resolved source apportionment of particulate matter in urban Beijing during haze and non-haze episodes. *Atmos Chem Phys* 16:1–19.
24. Quan J, et al. (2015) Effect of heterogeneous aqueous reactions on the secondary formation of inorganic aerosols during haze events. *Atmos Environ* 122:306–312.
25. Xie Y, et al. (2015) Enhanced sulfate formation by nitrogen dioxide: Implications from in situ observations at the SORPES station. *J Geophys Res* 120:12,679–12,694.
26. Li G, Zhang R, Fan J, Tie X (2005) Impacts of black carbon aerosol on photolysis and ozone. *J Geophys Res* 110:D23206.
27. Tie X, et al. (2003) Effect of clouds on photolysis and oxidants in the troposphere. *J Geophys Res* 108:4642.
28. Weber RJ, et al. (2016) High aerosol acidity despite declining atmospheric sulfate concentrations over the past 15 years. *Nat Geosci* 9(4):282–285.
29. Xu W, et al. (2014) Acid-catalyzed reactions of epoxides for atmospheric nanoparticle growth. *J Am Chem Soc* 136(44):15477–15480.
30. Wang L, et al. (2010) Atmospheric nanoparticles formed from heterogeneous reactions of organics. *Nat Geosci* 3:238–242.
31. Gomez-Hernandez M, et al. (2016) Hygroscopic characteristics of alkylaminium carboxylate aerosols. *Environ Sci Technol* 50(5):2292–2300.
32. Gomez ME, Lin Y, Guo S, Zhang R (2015) Heterogeneous chemistry of glyoxal on acidic solutions. An oligomerization pathway for secondary organic aerosol formation. *J Phys Chem A* 119(19):4457–4463.
33. Zhang R, Wooldridge PJ, Molina MJ (1993) Vapor-pressure measurements for the $H_2SO_4/HNO_3/H_2O$ and $H_2SO_4/HCl/H_2O$ Systems - incorporation of stratospheric acids into background sulfate aerosols. *J Phys Chem* 97:8541–8548.
34. Zhang R, Leu MT, Keyser LF (1996) Heterogeneous chemistry of HONO on liquid sulfuric acid: A new mechanism of chlorine activation on stratospheric sulfate aerosols. *J Phys Chem* 100:339–345.
35. Tursic J, Berner A, Podkrajsek B, Grgic I (2004) Influence of ammonia on sulfate formation under haze conditions. *Atmos Environ* 38:2789–2795.
36. Zhang R (2010) Atmospheric science. Getting to the critical nucleus of aerosol formation. *Science* 328(5984):1366–1367.
37. Zhang R, Khalizov A, Wang L, Hu M, Xu W (2012) Nucleation and growth of nanoparticles in the atmosphere. *Chem Rev* 112(3):1957–2011.
38. Qiu C, Zhang R (2013) Multiphase chemistry of atmospheric amines. *Phys Chem Chem Phys* 15(16):5738–5752.
39. Qiu C, Wang L, Lal V, Khalizov AF, Zhang R (2011) Heterogeneous reactions of alkylamines with ammonium sulfate and ammonium bisulfate. *Environ Sci Technol* 45(11):4748–4755.
40. Huang RJ, et al. (2014) High secondary aerosol contribution to particulate pollution during haze events in China. *Nature* 514(7521):218–222.
41. Zhang R, Leu MT, Keyser LF (1995) Hydrolysis of N_2O_5 and $ClONO_2$ on the $H_2SO_4/HNO_3/H_2O$ ternary solutions under stratospheric conditions. *Geophys Res Lett* 22:1493–1496.
42. Zhao J, Levitt NP, Zhang R, Chen J (2006) Heterogeneous reactions of methylglyoxal in acidic media: implications for secondary organic aerosol formation. *Environ Sci Technol* 40(24):7682–7687.
43. Levy M, et al. (2014) Measurements of nitrous acid (HONO) using ion drift-chemical ionization mass spectrometry during the 2009 SHARP field campaign. *Atmos Environ* 94:231–240.
44. Peng J, et al. (2016) Markedly enhanced absorption and direct radiative forcing of black carbon under polluted urban environments. *Proc Natl Acad Sci USA* 113(16):4266–4271.
45. Waller RE, Lawther PJ (1957) Further observations on London fog. *BMJ* 2(5059):1473–1475.
46. Wang Y, Zhang Q, He K, Zhang Q, Chai L (2013) Sulfate-nitrate-ammonium aerosols over China: Response to 2000–2015 emission changes of sulfur dioxide, nitrogen oxides, and ammonia. *Atmos Chem Phys* 13:2635–2652.
47. He H, et al. (2012) SO_2 over central China: Measurements, numerical simulations and the tropospheric sulfur budget. *J Geophys Res* 117:D00K37.
48. Liu X, et al. (2013) Enhanced nitrogen deposition over China. *Nature* 494(7438):459–462.
49. Pan Y, et al. (2016) Fossil fuel combustion-related emissions dominate atmospheric ammonia sources during severe haze episodes: Evidence from ^{15}N-stable isotope in size-resolved aerosol ammonium. *Environ Sci Technol* 50(15):8049–8056.
50. Suh I, Zhang R, Molina LT, Molina MJ (2003) Oxidation mechanism of aromatic peroxy and bicyclic radicals from OH-toluene reactions. *J Am Chem Soc* 125(41):12655–12665.
51. Zhao J, Zhang R, Misawa K, Shibuya K (2005) Experimental product study of the OH-initiated oxidation of m-xylene. *J Photoch Photobio A* 176:199–207.
52. Lei W, Zhang R, McGivern WS, Derecskei-Kovacs A, North SW (2001) Theoretical study of OH-O_2-isoprene peroxy radicals. *J Phys Chem* 105:471–477.
53. Lei W, Zhang R (2001) Theoretical study of hydroxy-isoprene alkoxy radicals and their decomposition pathways. *J Phys Chem* 105:3808–3815.
54. Wang GH, et al. (2014) Evolution of aerosol chemistry in Xi'an, inland China, during the dust storm period of 2013; Part 1: Sources, chemical forms and formation mechanisms of nitrate and sulfate. *Atmos Chem Phys* 14:11571–11585.
55. Rumsey IC, et al. (2014) An assessment of the performance of the Monitor for Aerosols and Gases in ambient air (MARGA): A semi-continuous method for soluble compounds. *Atmos Chem Phys* 14:5639–5658.
56. Nie W, et al. (2015) Influence of biomass burning on HONO chemistry in eastern China. *Atmos Chem Phys* 15:1147–1159.
57. Cao JJ, et al. (2003) Characteristics of carbonaceous aerosol in Pearl River Delta Region, China during 2001 winter period. *Atmos Environ* 37:1451–1460.
58. Cao JJ, et al. (2008) Size-differentiated source profiles for fugitive dust in the Chinese Loess Plateau. *Atmos Environ* 42:2261–2275.
59. Wang G, Huang L, Gao S, Gao S, Wang L (2002) Characterization of water-soluble species of PM10 and PM2.5 aerosols in urban area in Nanjing, China. *Atmos Environ* 36:1299–1307.
60. Hennigan CJ, et al. (2015) A critical evaluation of proxy methods used to estimate the acidity of atmospheric particles. *Atmos Chem Phys* 15:2775–2790.
61. Fortner EC, Zhao J, Zhang R (2004) Development of ion drift-chemical ionization mass spectrometry. *Anal Chem* 76(18):5436–5440.
62. Zheng J, et al. (2008) Measurements of HNO_3 and N_2O_5 using ion drift-chemical ionization mass spectrometry during the MCMA - 2006 campaign. *Atmos Chem Phys* 8:6823–6838.
63. Zhang R, Suh I, Lei W, Clinkenbeard AD, North SW (2000) Kinetic studies of OH-initiated reactions of isoprene. *J Geophys Res* 105:24627–24635.
64. Zhang R, Leu MT, Keyser LF (1994) Heterogeneous reactions involving $ClONO_2$, HCl, and HOCl on liquid sulfuric acid surfaces. *J Phys Chem* 98:13563–13574.

EARTH, ATMOSPHERIC, AND PLANETARY SCIENCES

Wang et al.